The American Journal of Pathology, Vol. 174, No. 1, January 2009

DOI: 10.2353/ajpath.2009.080573

Epithelial and Mesenchymal Cell Biology

Type XVII Collagen is a Key Player in Tooth Enamel Formation

Takuya Asaka,*† Masashi Akiyama,* Takanori Domon,‡ Wataru Nishie,* Ken Natsuga,* Yasuyuki Fujita,* Riichiro Abe,* Yoshimasa Kitagawa,† and Hiroshi Shimizu*

From the Department of Dermatology, Hokkaido University Graduate School of Medicine, Sapporo; Oral Diagnosis and Oral Medicine,† the Department of Oral Pathobiological Science, and the Division of Oral Functional Science,‡ the Department of Oral Functional Anatomy, Hokkaido University Graduate School of Dental Medicine, Sapporo, Japan*

Inherited tooth enamel hypoplasia occurs due to mutations in genes that encode major enamel components. Enamel hypoplasia also has been reported in junctional epidermolysis bullosa, caused by mutations in the genes that encode type XVII collagen (COL17), a component of the epithelial-mesenchymal junction. To elucidate the pathological mechanisms of the enamel hypoplasia that arise from the deficiency of epithelial-mesenchymal junction molecules, such as COL17, we investigated tooth formation in our recently established *Col17*$^{-/-}$ and *Col17* rescued mice. Compared with wild-type mice, the incisors of the *Col17*$^{-/-}$ mice exhibited reduced yellow pigmentation, diminished iron deposition, delayed calcification, and markedly irregular enamel prisms, indicating the presence of enamel hypoplasia. The molars of the *Col17*$^{-/-}$ mice demonstrated advanced occlusal wear. These abnormalities were corrected in the *Col17* rescued humanized mice. Thus, the *Col17*$^{-/-}$ mice clearly reproduced the enamel hypoplasia in human patients with junctional epidermolysis bullosa. We were able to investigate tooth formation in the *Col17*$^{-/-}$ mice because the *Col17*$^{-/-}$ genotype is not lethal. *Col17*$^{-/-}$ mouse incisors had poorly differentiated ameloblasts that lacked enamel protein-secreting Tomes' processes and reduced mRNA expression of amelogenin, ameloblastin, and of other enamel genes. These findings indicated that COL17 regulates ameloblast differentiation and is essential for normal formation of Tomes' processes. In conclusion, COL17 deficiency disrupts the epithelial-mesenchymal interactions, leading to both defective ameloblast differentiation and enamel malformation. ***(Am J Pathol 2009, 174:91–100; DOI: 10.2353/ajpath.2009.080573)***

Mesenchymal-epithelial interactions are thought to play essential roles in development of epithelial organs including the epidermis, hair follicles, and teeth. A variety of soluble factors, cell surface markers, and signal molecules have been reported to be involved in mesenchymal-epithelial interactions.[1,2] The hemidesmosome is a subcellular junctional adhesion structure overlying the basement membrane between the mesenchyme and epithelial cells that binds the epithelial cells to the underlying mesenchymal tissue.[3] Type XVII collagen (COL17) previously called "bullous pemphigoid antigen 2" or "BP180," is a transmembrane glycoprotein expressed in stratified and complex epithelia, such as the skin, the mucous membrane, and the eye, where it plays a crucial role in hemidesmosome stability and epithelial-mesenchymal attachment.[4]

Non-Herlitz junctional epidermolysis bullosa (nH-JEB) caused by COL17 deficiency shows the abnormal tooth formation of amelogenesis imperfecta.[5–7] We therefore hypothesized that COL17 in hemidesmosomes also plays an important role in mesenchymal-epithelial interactions in tooth formation.

Enamel formation is easily disrupted and enamel defects may reflect more than just genetic abnormalities. Enamel defects can also be attributed to environmental factors that cause chronological hypoplasia of the enamel during the enamel formation period.[7] It is important to study the pathomechanisms of enamel malformation in mice with defects in hemidesmosome components. There are several model mice with epithelial mesenchymal junction (EMJ) component deficiencies.[3,8] Among them, only laminin332-deficient mice are expected to have tooth malformation. However, the laminin332 knockout mice are

Supported in part by Grant-in-Aid from the Ministry of Education, Science, Sports and Culture of Japan to M. Akiyama (Kiban 20390304).

Accepted for publication September 30, 2008.

Address reprint requests to Masashi Akiyama, M.D., Ph.D., Department of Dermatology, Hokkaido University Graduate School of Medicine, North 15 West 7, Kita-ku, Sapporo 060-8638, Japan. E-mail: akiyama@med.hokudai.ac.jp.

lethal in their early development and tooth abnormality in adult mice has not been examined sufficiently.[8]

The *Col17* knockout (*Col17*$^{-/-}$) mice that we established recently are not lethal at birth; thus, we can use them to investigate the pathomechanisms of enamel defects that arise from hemidesmosome component deficiency.

To clarify the roles of COL17 in tooth formation, we studied the detailed process of tooth formation in *Col17* knockout (*Col17*$^{-/-}$) mice, which we recently established.[9] We show that COL17 has a critical role in tooth formation, especially in the differentiation of ameloblasts and enamelization, suggesting the importance of junction structure in mesenchymal-epithelial interaction during tooth formation.

Materials and Methods

Generation of *Col17*$^{-/-}$ Mice and Rescued COL17-Humanized Mice

The procedure for generating COL17$^{-/-}$ mice has been described.[9] Briefly, we cloned a 14.7-kb mouse genomic DNA COL17 fragment from the mouse 129Sv/Ev genomic library (Stratagene, La Jolla, CA). We subcloned a 11.5-kb *Nhe*I to *Not*I fragment to make the targeting vector. We inserted the PGK/Neo cassette between 6-bp upstream of the ATG start codon in exon 2 and 1.2-kb downstream in intron 2. We transfected the targeting vector by electroporation into 129 Sv/Ev embryonic stem cells, then microinjected the correctly targeted embryonic stem cell line into blastocysts obtained from C57BL/6J mice (Jackson Laboratory, Bar Harbor, Maine) to generate chimeric mice, which we then mated with C57BL/6J females. We crossed F1 heterozygotes with C57BL/6J for more than four generations and then intercrossed them to generate *Col17*$^{-/-}$ mice. The procedures for screening *Col17*$^{-/-}$ mice by PCR, reverse transcription (RT)-PCR, Northern and Western blotting, histology, electron microscopy, and immunofluorescence are described elsewhere.[9]

The phenotypic features of the *Col17* knockout (*Col17*$^{-/-}$) mice closely resembled those seen in nH-JEB (OMIM: 226650) caused by null mutations in the *COL17A1* gene, as previously described.[9] The *Col17*$^{-/-}$ mice had skin blisters and erosions from mild trauma. *Col17*$^{-/-}$ mice skin showed subepidermal blistering associated with a lack of COL17 and poorly formed hemidesmosomes.

Procedures for generating COL17-rescued mice have been described elsewhere.[9] Briefly, we crossed transgenic mice (C57BL/6 background) expressing the squamous epithelium-specific K14 promoter and a human *COL17* cDNA (*Col17*$^{m+/+}$, *COL17*$^{h+}$) with heterozygous *Col17*$^{m+/-}$ mice. Mice that carried both the heterozygous null mutation of *Col17* and the transgene of human *Col17* (*Col17*$^{m+/-}$, *COL17*$^{h+}$) were bred to produce rescued *Col17*$^{m-/-}$, *COL17*$^{h+}$ COL17-humanized mice.

The rescued mice showed almost none of the abnormal manifestations seen in the *Col17*$^{-/-}$ mice.[9]

Structural Analysis of Mouse Dentition

Tissue samples of mice were incubated in hot (approximately 90°C) distilled water for several minutes, and soaked in 10% Tasinase (Kyowa-hakkou, Tokyo, Japan) at 37°C for 6 hours. Incisors and first molars were taken from maxillomandibular tissue by removal of soft tissue. The teeth were carefully cleaned and were observed macroscopically. After air-drying overnight, the teeth were sputter-coated with carbon CC-40F (Meiwa-shouji, Osaka, Japan), and were observed with a Hitachi S-4000 scanning electron microscope (Hitachi Electronics, Tokyo, Japan) operated at 15 kV. For the observation of enamel rod inclination, sagittal sections of maxillary incisors were etched by a grinder for 30 seconds in 0.1N hydrochloric acid and were observed similarly.

Chemical and Mineralization Analyses

Qualitative and distributive elemental analysis was performed in sagittal sections of maxillary incisors prepared with a grinder and in the labial side of maxillary incisors with a Hitachi S-2380 scanning electron microscope (Hitachi, Tokyo, Japan) operated at 15kV and energy dispersive X-ray spectrometry (EDX).

To demonstrate the patterns of mineralization, radio transparencies of the contact microradiographs were examined as previously described.[10] Maxillary incisors were dehydrated by passage through a series of ascending concentrations of ethanol solutions and embedded in polyester resin (Rigolic, Ouken Co., Tokyo, Japan). Longitudinal labio-lingual ground sections of 100-μm thickness were prepared with a rotary diamond saw (Speadrap ML521; Maruto, Tokyo, Japan) and emery papers. Microradiographs of the ground sections were recorded on Kodak SO-181 high-resolution film (Eastman Kodak, Rochester, NY) using a cabinet X-ray apparatus (CSM-2; Softex, Tokyo, Japan) at 15 kV, 4 mA for 20 minutes. The films were developed, fixed, and observed under a light microscope.

Preparation of Tissue Sections and Immunohistochemistry

Under anesthesia with ether inhalation, intracardiac perfusions for 2-week-old mice were performed with a fixative solution containing 4% paraformaldehyde in PBS, pH 7.4. Postfixation was ensured by immersion of dissected maxilla and mandible in the fixative solution overnight at 4°C.

The maxillae and mandibles with incisors were processed for histological analysis by decalcification at 4°C for up to 2 weeks in a pH 7.4 PBS solution containing 10% EDTA. After extensive washing in PBS, the samples were dehydrated in increasing concentrations of ethanol and lemosol (Wako, Osaka, Japan), and were finally embedded in paraffin. Serial longitudinal and frontal sections of the incisors of the paraffin-embedded specimens (5 μm) were processed for H&E staining.

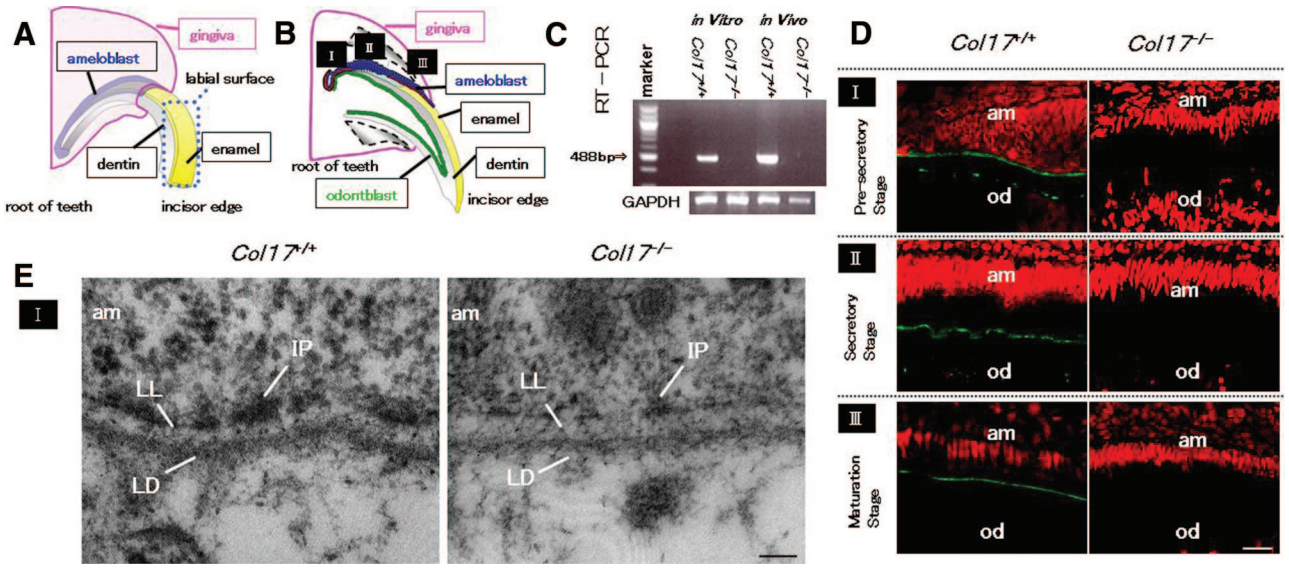

Figure 1. COL17 expression in the tooth of *Col17*$^{+/+}$ mice and COL17 absence in the tooth of *Col17*$^{-/-}$ mice. **A, B:** Mouse incisors are continuously elongating teeth. In the root of these incisors, ameloblasts (blue) and odontoblasts (green) secrete enamel matrix and dentin, respectively, during the secretory stage (II). I: the pre-secretory stage; II: the secretory stage; III: the maturation stage. **C:** A RT-PCR assay revealed that *Col17* mRNA (488 bp band) was expressed in cultured ameloblasts from *Col17*$^{+/+}$ mice (**left lane**) and *Col17*$^{+/+}$ mouse teeth (**second right**). *Col17* mRNA was not expressed in cultured ameloblasts from *Col17*$^{-/-}$ mice (**second left lane**) or *Col17*$^{-/-}$ mouse teeth (**right hand lane**). **D:** Immunofluorescence staining for COL17 (green) revealed that COL17 was expressed in the EMJ between ameloblasts and odontoblasts at the pre-secretory stage of a *Col17*$^{+/+}$ mouse (**upper, left**), between ameloblasts and enamel matrix in the secretory stage (**middle, left**) and in the maturation stage (**lower, left**) of a *Col17*$^{+/+}$ mouse. At the secretory stage, COL17 expression was weak, intermittent, or absent. In *Col17*$^{-/-}$ mice, no COL17 staining was observed in the EMJ at any stage (**right column**). am: ameloblast; od: odontblast. Scale bar = 20 μm. **E:** Ultrastructural features of the basement membrane zone at the pre-secretory stage. Normal hemidesmosomes were seen in the *Col17*$^{+/+}$ mouse (**left**), but hypoplastic, malformed hemidesmosomes were observed in the *Col17*$^{-/-}$ mice (**right**). am: ameloblast; LL: lamina lucida; IP: inner attachment plaques; LD :lamina densa. Scale bar = 60 nm.

For immunohistochemistry, neonatal mice (day-1) were sacrificed and the tissue samples were embedded in optimal cutting temperature compound (Sakura Finetechnical Co., Tokyo, Japan) for frozen sectioning. Frozen tissue sections were cut at a thickness of 6 μm sagittally until incisors were exposed, or coronally until molars were exposed. Sections were fixed with acetone for 10 minutes at −20°C, and washed in PBS, incubated with a primary antibody, anti-mouse COL17 monoclonal antibody (NC-16A, final dilution, 1:2500), at 37°C for 30 minutes. Then, the sections were incubated with a secondary antibody, fluorescein isothiocyanate (FITC)-conjugated goat anti-rat IgG (H+L; Jackson ImmunoResearch Laboratories, Suffolk, UK; final dilution, 1:50), at 37°C for 30 minutes, and incubated with 10 μg/ml of propidium iodide at 37°C for 10 minutes for nuclear counterstaining. Sections were observed under an Olympus Fluoview confocal laser-scanning microscope (Olympus, Tokyo, Japan).

Ultrastructural Analysis during Tooth Formation

As above, from the maxillomandibular tissue fixed with modified Karnovsky's fixative (at a final concentration of 2% paraformaldehyde and 2.5% glutaraldehyde in 0.05 mol/L cacodylate buffer solution, pH 7.4), 2-week-old mice incisors were obtained and decalcified in 10% EDTA pH 7.4, at 4°C for 2 weeks. After decalcification, samples were postfixed in 1% osmium tetroxide at 4°C for 2 hours and stained *en bloc* with 1% uranyl acetate at 4°C for 20 minutes. The samples were dehydrated through a graded series of ethanol and embedded in Epon 812 (TAAB Laboratories, Berkshire, UK). Ultrathin sections were cut in the sagittal direction to include both the separated enamel organ and the dental papilla. Sections were stained with uranyl acetate and lead citrate, and observed under a Hitachi H-7000 transmission electron microscope (Hitachi, Tokyo, Japan).

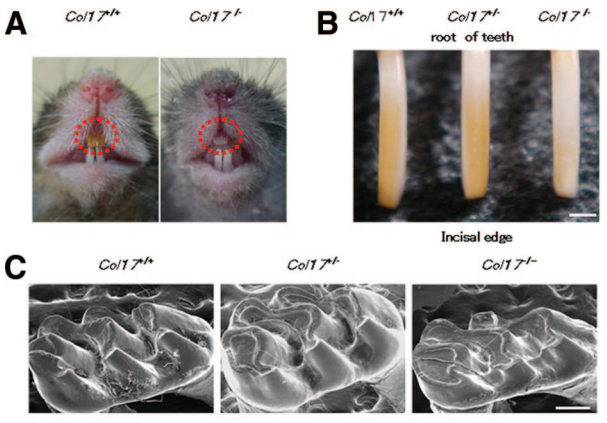

Figure 2. Dental phenotype of *Col17*$^{-/-}$ mice. **A:** At 4 weeks of age, a *Col17*$^{-/-}$ mouse (**right**) had whitish incisors. **B:** Incisors from *Col17*$^{+/+}$ and *Col17*$^{+/-}$ mice showed yellowish color, although an incisor from a *Col17*$^{-/-}$ mouse seemed whitish (**right**). Scale bar = 500 μm. **C:** In the molars, tooth wear was more advanced for the *Col17*$^{-/-}$ mice (**right**) than for the *Col17*$^{+/+}$ (**left**) and *Col17*$^{+/-}$ (**center**) mice. Scale bar = 250 μm.

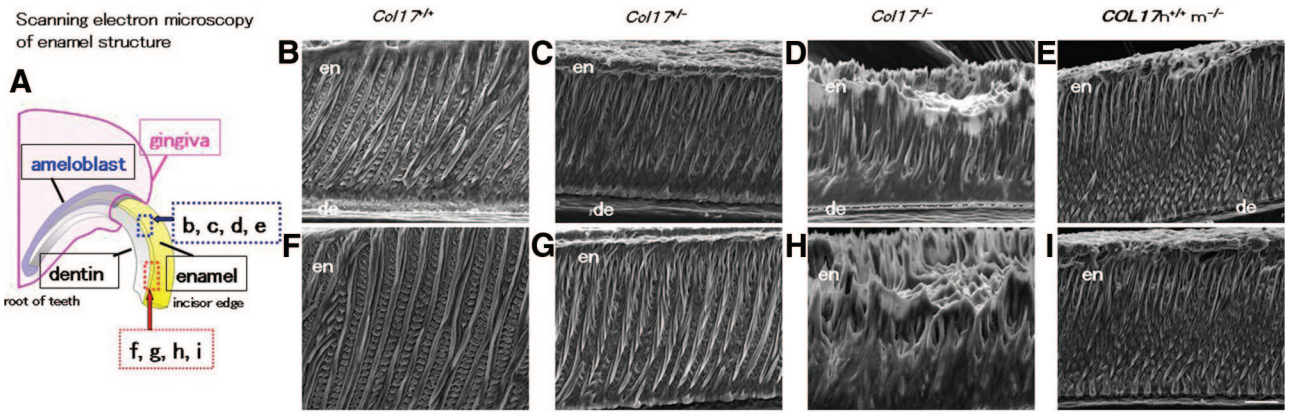

Figure 3. Scanning electron microscopy of the sagittal section of maxillary incisors. **A:** A model of an upper incisor. The enamel layer indicated by an **upper blue rectangle** and by a **lower red rectangle** is enlarged in **B**, **C**, **D** and **E**, and in **F**, **G**, **H** and **I**, respectively. In the *Col17*$^{-/-}$ mouse, irregular inclinations of enamel rods without a normal network arrangement are observed (**D**, **H**), in contrast to the regular network of enamel rods observed in the *Col17*$^{+/+}$ incisor (**B**, **F**) and in the *Col17*$^{+/-}$ incisor (**C**, **G**). The normal, regular network of enamel rods has been restored in the COL17 humanized mouse (**E**, **I**). en: enamel; de: dentin. Scale bar = 20 μm.

Terminal Deoxynucleotidyl Transferase-Mediated dUTP Nick-End Labeling Staining

For the detection of apoptotic cells in the ameloblast layer by terminal deoxynucleotidyl transferase-mediated dUTP nick-end labeling (TUNEL) assay, paraffin sections were processed with *in situ* apoptosis detection kits (Apoptag; Chemicon International, Temecula, CA).[11] The number of apoptotic ameloblasts at each stage was calculated based on the criterion that an apoptotic body of more than 2 μm in diameter could be defined as a count; these numbers were compared between *Col17*$^{+/+}$ and *Col17*$^{-/-}$.

Cell Cultures and Immunolabeling

For dental epithelial cell cultures, maxillary and mandibular incisors from 2-week-old mice were dissected, and the distal part of the incisors was removed. Tooth samples were treated with 0.25% trypsin for 10 minutes and pipetted up and down intensely. The dental epithelial cells, dental mesenchymal cells, and various other cells were isolated from incisors. To separate dental epithelial cells from the other cells, cells were cultured in epidermal keratinocyte medium containing a small amount of bovine pituitary extract (CNT-57; CELLnTEC Advanced Cell Systems, Bern, Switzerland) for 7 days. After obtaining a sufficient number of dental progenitor epithelial cells, we changed the culture medium to epidermal keratinocyte medium containing 0.07 mmol/L calcium (CNT-02; CELLnTEC Advanced Cell Systems, Bern, Switzerland) to induce differentiation, and cultured it for 10 days.

For fluorescence staining, the cells were fixed with 70% ethanol for 10 minutes and washed with PBS. The cells were incubated with a primary antibody anti-mouse amelogenin polyclonal antibody (Hokudo, Sapporo, Japan), final dilution of 1:100 or with anti-mouse ameloblastin polyclonal antibody (Santa Cruz Biotechnology, Santa Cruz, CA), final dilution, 1:50, at 37°C for 30 minutes. Then, the cells were incubated with the secondary antibody FITC-conjugated goat anti-rabbit IgG (H+L; Jackson ImmunoResearch Laboratory, West Grove, PA), final dilution, 1:50, or with FITC-conjugated donkey anti-goat IgG (H+L; Jackson ImmunoResearch Laboratory, West Grove, PA), final dilution, 1:50, at 37°C for 30 minutes and incubated with 10 μg/ml of propidium iodide at 37°C for 10 minutes to visualize the nucleus. The cells were observed under an Olympus FluoView confocal laser-scanning microscope (Olympus, Tokyo, Japan).

RT-PCR Analysis

To study *Col17* mRNA expression in dental epithelial cells and ameloblasts, total RNA from incisors or cultured dental epithelial cells was extracted using TRIZOL reagent (Invitrogen, Carlsbad, CA), according to the manufacturer's instructions. Extracted RNA was used for cDNA synthesis in SuperScript III reverse transcriptase (Invitrogen, Carlsbad, CA) according to the manufacturer's instructions. The following primers specific for mouse *Col17* sequence (NM: 007732) were used for RT-PCR: 5′-AGAAGAAAA GCATCCGAGGG-3′ (RT-F); and 5′-TGGTTGAAGAAGAGGCGAGT-3′ (RT-B). As a control, we used the primers for mouse glyceraldehyde-3-phosphate dehydrogenase (GAPDH; NM: 001001303): 5′-TTAGCCCCCCTGGCCAAGG-3′ (mGAPDH-F) and 5′-CTTACTCCTTGGAGGCCATG-3′ (mGAPDH-B), which amplified a 541-bp fragment.

Real-Time RT-PCR Analysis

To quantitatively analyze mRNA expression levels of tooth-formation-associated proteins, amelogenin, ameloblastin, enamelin, tuftelin, enamelysin, and dentin sialophosphoprotein (DSPP), in teeth from the *Col17*$^{+/+}$ and *Col17*$^{-/-}$ mice, cDNA samples were analyzed using the ABI prism 7000 sequence detection system (Applied Biosystems, Foster City, CA). Primers and probes specific for amelogenin, ameloblastin, enamelin, tuftelin, enamelysin, DSPP, and control housekeeping genes, GAPDH and β-ac-

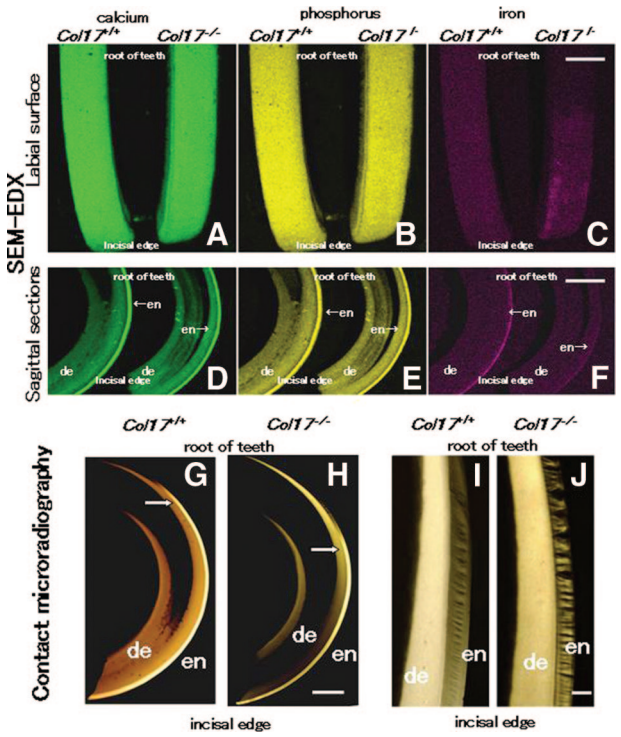

Figure 4. Difference in enamel formation between *Col17*$^{+/+}$ and *Col17*$^{-/-}$ mice incisors. The labial surface (see Figure 1A) is featured in **A**, **B**, and **C**. A sagittal section is shown in **D**, **E**, and **F**. **A, B:** The labial surface of the maxillary incisors in both *Col17*$^{+/+}$ (**left**) and *Col17*$^{-/-}$ (**right**) mice was scanned for calcium (green) and phosphorus (yellow) with EDX spectrometry. No obvious difference was observed in elemental distribution mapping. **C:** The same surfaces scanned in EDX for iron (red). In *Col17*$^{-/-}$ mice (**right**), the distribution of iron was irregular, compared with that of a *Col17*$^{+/+}$ mice (**left**). Scale bar: (**A, B, C**) = 500 μm. **D, E, F:** The sagittal sections of the maxillary incisors of both *Col17*$^{+/+}$ (**left**) and *Col17*$^{-/-}$ (**right**) mice scanned in EDX for calcium (green), phosphorus (yellow), and iron (red). No obvious difference is observed in the distribution of calcium or phosphorus between the *Col17*$^{+/+}$ (**left**) and *Col17*$^{-/-}$ (**right)** mice. In the *Col17*$^{-/-}$ mice (**right**), the iron concentration in the enamel is lower than that in the *Col17*$^{+/+}$ mouse (**left**; **F**). en: enamel; de: dentin. Scale bars in (**D, E, F**) = 1000 μm. **G, H:** Microradiographs of maxillary incisors in *Col17*$^{+/+}$ (**G**) and *Col17*$^{-/-}$ (**H**) mice. The position (**arrows**) where sufficient mineralization occurred in the enamel judged from the low radio-opacity signal, moved toward the incisal edge in maxillary incisors of a *Col17*$^{-/-}$ mouse (**G**), compared with that in incisors of a *Col17*$^{+/+}$ mouse (**H**). en: enamel; de: dentin. Scale bar: (**G, H**) = 500 μm. **I, J:** Microradiographs showing the mineralization pattern of the developing enamel at the maturation stage from *Col17*$^{+/+}$ (**I**) and *Col17*$^{-/-}$ (**J**) mice. As compared with *Col17*$^{+/+}$ (**I**), the mineralization demonstrated by radio-opacity of the enamel was irregular in both stages in *Col17*$^{-/-}$ mice (**J**), although there were no differences in the radio-opacity of dentine between *Col17*$^{+/+}$ (**I**) and *Col17*$^{-/-}$ (**J**) mice. en: enamel; de: dentin. Scale bar: (**I, J**) = 100 μm.

tin, were obtained from the TaqMan gene expression assay (Applied Biosystems, Foster City, CA; Probe ID; Mm00711644_g1, Mm00477485_m1, Mm00516922_m1, Mm00449139_m1, Mm00600244_m1 and Mm00515666_m1, Mm99999915_gl, Mm00607939_sl).

Differences between the mean CT values of mRNA expressions of tooth-formation-associated proteins and those of GAPDH or ß-actin were calculated as $\triangle CT_{Col17-/-\ mice} = CT_{tooth\ protein} - CT_{GAPDH\ (or\ other\ housekeeping\ genes)}$ and those of $\triangle CT$ for the *Col17*$^{+/+}$ incisors as $CT_{calibrator} = CT_{tooth\ protein} - CT_{GAPDH\ (or\ other\ housekeeping\ genes)}$. Final results for *Col17*$^{-/-}$ incisor samples/*Col17*$^{+/+}$ incisor samples (%) were determined by $2^{-(CT\ Col17-/-\ -\ CTcalibrator)}$.

Using similar methods, we quantitatively analyzed the tooth-formation-associated protein mRNA expression levels in the dental epithelial cells cultured from the *Col17*$^{+/+}$ and *Col17*$^{-/-}$ mice.

Results

COL17 Expression Pattern in the EMJ of Teeth in *Col17*$^{-/-}$ Mice

We observed the expression of *Col17* at each of the three stages of enamel formation: pre-secretory, secretory, and maturation (Figure 1, A and B). The 488-bp fragments of mouse *Col17* mRNA were detected in *Col17*$^{+/+}$ mouse incisors *in vivo* and in cells cultured from *Col17*$^{+/+}$ mouse incisors *in vitro*, although mouse *Col17* mRNA was detected in neither incisors nor cultured cells from *Col17*$^{-/-}$ mice (Figure 1C).

To clarify COL17 expression during tooth formation, we immunostained tissue sections of maxillary incisors in which we could observe all differentiation stages of tooth formation. COL17 was expressed in the EMJ between ameloblasts and odontoblasts at the pre-secretory stage. Due to elongation of Tomes' processes, the basement membrane became discontinuous and COL17 expression was reduced and in places became intermittent at the secretory stage. COL17 expression reappeared at the maturation stage (Figure 1D).

In the *Col17*$^{-/-}$ mice, COL17 expression was not observed in the EMJ under the ameloblasts at any stage during tooth development.

The basement membrane on the basal surface of the ameloblasts separates the ameloblasts from mesenchymal tissue/pre-odontoblasts. Hemidesmosomes are observed in the EMJ, and they are composed of prominent inner plaques, outer plaques, and sub-basal dense plates, similar to those in the dermo-epidermal junction in the skin. Anchoring filaments cross the lamina lucida, and anchoring fibrils anchor lamina densa to the mesenchymal tissue in the *Col17*$^{+/+}$ mice (Figure 1E).

In the *Col17*$^{-/-}$ mice, there were a reduced number of hypoplastic inner and outer hemidesmosomal attachment plaques with poor keratin filament association and less prominent anchoring filaments, whereas anchoring fibrils and the lamina densa were both normally preserved (Figure 1E).

Dental Phenotype in the *Col17*$^{-/-}$ Mice

The incisors of wild-type (*Col17*$^{+/+}$) and heterozygous (*Col17*$^{+/-}$) mice exhibit yellow pigmentation on the surface. The incisors of the *Col17*$^{-/-}$ mice had a chalky, whitish appearance (Figure 2, A and B). The *Col17*-rescued mice (mouse *Col17*$^{-/-}$, human *COL17*$^{+/+}$) had yellowish incisors, as did the wild-type *Col17*$^{+/+}$ mice (data not shown). By scanning electron microscopy, the enamel surface of the *Col17*$^{+/+}$, *Col17*$^{+/-}$ and *Col17*$^{-/-}$ mice appeared smooth and unpitted (data not shown). Molar wear was more advanced in the *Col17*$^{-/-}$ mice than in the *Col17*$^{+/+}$ and *Col17*$^{+/-}$ mice. This tooth wear

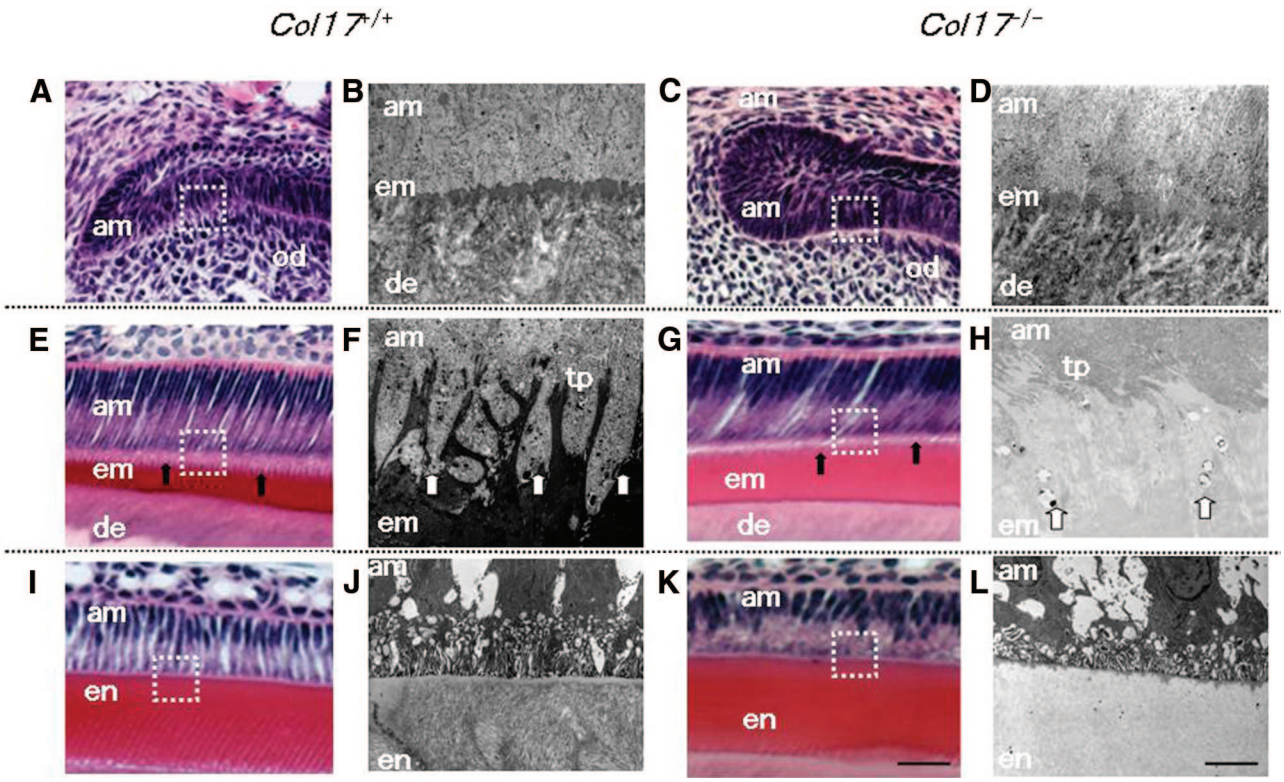

Figure 5. Malformed Tomes' processes and defective amelogenesis in *Col17*$^{-/-}$ mice **A–D:** At the pre-secretory and early secretory stages, the EMJ separates pre-ameloblasts and pre-odontoblasts. **A, C:** The overall structures of pre-ameloblasts and pre-odontoblasts were similar in the *Col17*$^{+/+}$ (**A**) and *Col17*$^{-/-}$ (**C**) mice in the pre-secretory to the early secretory stages at the light microscopic level. **B, D:** Ultrastructurally, from the pre-secretory to the early secretory stages, the basement membrane between ameloblasts and odontoblasts was blurred in the *Col17*$^{-/-}$ mouse (**D**), compared with more obvious, intact basement membrane structures in a *Col17*$^{+/+}$ mouse (**B**). **E–H:** At the secretory stage, Tomes' processes are formed and enamel matrix is produced by ameloblasts. **E, G:** In the secretory stage, the processes of ameloblasts were malformed and blurred (**arrows**) in the *Col17*$^{-/-}$ mouse (**G**), compared with well-organized lattice-like structures of the Tomes' processes (**arrows**) in the *Col17*$^{+/+}$ mice (**E**). The thickness of the enamel matrix seemed similar both in *Col17*$^{+/+}$ (**E**) and *Col17*$^{-/-}$ (**G**) mice. At the secretory stage, Tomes' processes were apparently hypoplastic in the *Col17*$^{-/-}$ mouse (**H**), compared with normal Tomes' processes in the *Col17*$^{+/+}$ mouse (**F**). **I–L:** In the maturation stage, disruption of the processes of ameloblasts (am) was more advanced in the *Col17*$^{-/-}$ mouse (**K**), compared with regular processes in the *Col17*$^{+/+}$ mice (**I**). At the maturation stage, the electron density of the enamel matrix is remarkably lower in the *Col17*$^{-/-}$ mouse (**L**) than that in the *Col17*$^{+/+}$ mouse (**J**). In addition, enamel rod structures are blurred in the enamel matrix of the *Col17*$^{-/-}$ mouse (**L**). am: ameloblast; em: enamel matrix; en: enamel; de: dentin; od: odontoblast; tp: Tomes' processes. Scale bars: (**A, C, E, G, I, K**) = 30 μm; (**B, D, F, H, J, L**) = 3 μm.

became more severe with age, although it failed to extend to loosen the molar crown (Figure 2C). In sagittal sections of the *Col17*$^{-/-}$ mice maxillary incisors, the enamel rod inclination was irregularly oriented and disrupted and had lost its normal network arrangement seen in that of *Col17*$^{+/+}$ and *Col17*$^{+/-}$ mice (Figure 3 A–D, F–H). In the COL17-rescued mouse *Col17*$^{-/-}$, human *COL17*$^{+/+}$ mice, the maxillary incisors showed normal enamel rod formation (Figure 3, E and I) confirming that the enamel changes were caused by a Col17 deficiency.

Chemical and Mineralization Analysis of the Teeth

Backscatter electron images of the labial surface and the sagittal sections of the maxillary incisors in the *Col17*$^{+/+}$, *Col17*$^{+/-}$, and *Col17*$^{-/-}$ mice revealed that calcium and phosphorus were homogeneously distributed from incisal edge to apical root in all samples (Figure 4A, B, D, E). In the *Col17*$^{+/+}$ and *Col17*$^{+/-}$ mice, iron was lightly but uniformly distributed from incisal edge to the middle of teeth, and the density corresponded with the yellow pigmentation. In the *Col17*$^{-/-}$ mice, iron was irregularly distributed (Figure 4, C and F).

To compare the mineralization patterns of teeth between the *Col17*$^{+/+}$ and *Col17*$^{-/-}$ mice, radio transparencies of the microradiographs were examined in maxillary incisors. The radio-opacity of enamel decreased gradually toward the incisal edge, from the enamel secretory stage to the maturation stage. Mineralization reached its maximum during the late maturation stage (Figure 4G). To objectively evaluate the mineralization level in the enamel layers, we set up a marker-point for enamel matrix sufficiently completed mineralization using image analysis. The point exhibited 90% or more saturation levels in the completely mineralized incisal edge-side of enamel layer. We then assessed each image for the area that showed this or higher saturation signals. The mineralization marker-points that we defined were at 1.7 mm and 2.7 mm from the incisor root in the *Col17*$^{+/+}$ mice and *Col17*$^{-/-}$ mice, respectively (Figure 4H). These findings indicated that, in the *Col17*$^{-/-}$ incisors, mineralization of enamel was delayed by 1.0 mm toward the incisal edge compared with that of the

Col17$^{+/+}$ incisors. Mineralization of the enamel matrix, at the maturation stage, was irregular and discontinuous in the *Col17*$^{-/-}$ mice (Figure 4I) compared with the *Col17*$^{+/+}$ mice (Figure 4J).

Defective Amelogenesis in Col17$^{-/-}$ *Mice*

Ameloblast size and the enamel matrix thickness in the *Col17*$^{-/-}$ mice were similar to those in the *Col17*$^{+/+}$ mice. The Tomes' processes of the *Col17*$^{+/+}$ mice were triangular and arranged in order. However, the processes of the *Col17*$^{-/-}$ mice were deformed and difficult to clearly visualize in H&E-stained sections (Figure 5A, C, E, G, I, K).

Furthermore, we observed enamel formation of the incisors of the *Col17*$^{+/+}$, *Col17*$^{+/-}$, and *Col17*$^{-/-}$ mice ultrastructurally. Secretory ameloblasts were tall columnar cells with intact Tomes' processes producing enamel matrix in the *Col17*$^{+/+}$ and *Col17*$^{+/-}$ mice (Figure 5, B and D).

In the *Col17*$^{-/-}$ mice, the Tomes' processes were thin, fragmented and disorganized, showing a wavy, villous appearance. There was no obvious difference in the other structural components of the ameloblasts (Figure 5, F and H).

Mature ameloblasts were columnar cells and could be divided into ruffle-based ameloblasts and smooth-ended ameloblasts by the presence of a ruffled border. Rough endoplasmic reticulum, lysosomes, mitochondria, small vacuoles and Golgi apparatus were seen in the apical and mid portions of mature ameloblasts. The cell structure and organelles of *Col17*$^{-/-}$ mature ameloblasts appeared normal, but the enamel rods were malformed and irregularly distributed. The electron density of the enamel matrix was remarkably low during the secretory and maturation stages in the *Col17*$^{-/-}$ mice, compared with the high electron density of the enamel matrix in the *Col17*$^{+/+}$ and *Col17*$^{+/-}$ mice (Figure 5, J and L).

Assay of Ameloblast Proliferation and Differentiation

Colony-forming analysis revealed there was no significant difference in colony-forming ability of cultured ameloblasts between the Col17$^{+/+}$ and Col17$^{-/-}$ mice (data not shown). As for apoptosis, TUNEL staining did not reveal excessive apoptosis of ameloblasts at the pre-secretory to secretory stages in either the Col17$^{+/+}$ or the Col17$^{-/-}$ mice (data not shown).

TUNEL assays showed that some apoptotic cells appeared from the late secretory stage to the early maturation stage (called the "transitional stage") of the *Col17*$^{+/+}$ and *Col17*$^{-/-}$ mice (data not shown). However, there was no significant difference in the number of TUNEL-positive cells between *Col17*$^{+/+}$ and *Col17*$^{-/-}$ mice; in the numbers of apoptotic ameloblasts per sagittal incisor section, 7.5 ± 0.7 cells/sagittal section in *Col17*$^{+/+}$ incisors and 7.0 ± 1.0 cells/sagittal section in *Col17*$^{-/-}$ incisors.

We examined the expression of enamel proteins in the incisors *in vivo* and in cultured dental epithelial cells *in vitro* using real-time RT-PCR analysis.[12–14] mRNA expression of the major enamel proteins produced by ameloblasts, including amelogenin, ameloblastin, enamelin, enamelysin, and DSPP, was significantly decreased in the *Col17*$^{-/-}$ incisors, except for the expression of tuftelin (Figure 6A). Tuftelin expression was only slightly reduced in *Col17*$^{-/-}$ mice incisors. In dental epithelial cells cultured from the *Col17*$^{+/+}$ mice, mRNA expression of amelogenin, ameloblastin, enamelin, and tuftelin was confirmed, although mRNA expression of enamelysin and DSPP was absent. In the *Col17*$^{-/-}$ mice, mRNA expression of amelogenin, ameloblastin and enamelin in cultured cells were remarkably lower than in the *Col17*$^{+/+}$ mice. Tuftelin expression was higher than that in the cells cultured from the *Col17*$^{+/+}$ mice (Figure 6B). Immunocy-

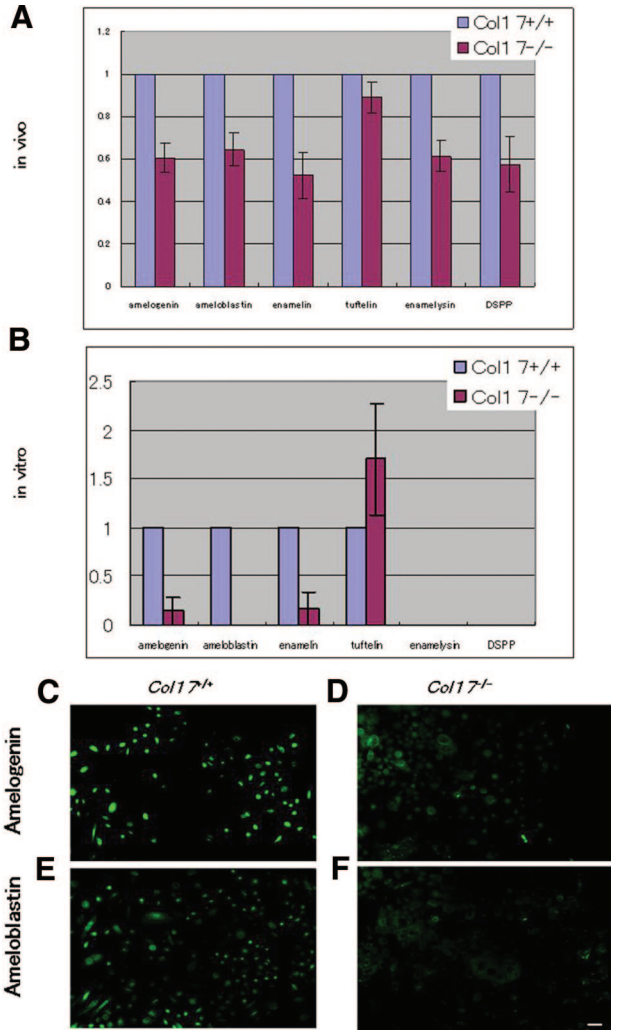

Figure 6. Expression of enamel proteins in *Col17*$^{-/-}$ ameloblasts. **A:** mRNA expression of all of the enamel proteins examined (amelogenin, ameloblastin, enamelin, tuftelin, enamelysin, and DSPP) was down-regulated in ameloblasts of incisors of the *Col17*$^{-/-}$mice *in vivo*. **B:** *In vitro* ameloblasts cultured from incisors of the *Col17*$^{-/-}$ mice showed down-regulated mRNA expression of amelogenin, ameloblastin and enamelin, although tuftelin expression was up-regulated relative to tuftelin expression of the cultured ameloblasts from the *Col17*$^{+/+}$ mice. Neither enamelysis nor DSPP was expressed in ameloblasts cultured from the *Col17*$^{+/+}$ and *Col17*$^{-/-}$ mice. **C:** Protein expression (FITC, green) of amelogenin and ameloblastin was decreased in ameloblasts cultured from the *Col17*$^{-/-}$ mice (**D, F**), relative to that in ameloblasts cultured from the *Col17*$^{+/+}$ mice (**C, E**). (**C, D**) amelogenin staining; (**E, F**) ameloblastin staining; (**C, E**) cells from *Col17*$^{+/+}$ mice; (**D, F**) cells from *Col17*$^{-/-}$ mice. Scale bar = 20 μm.

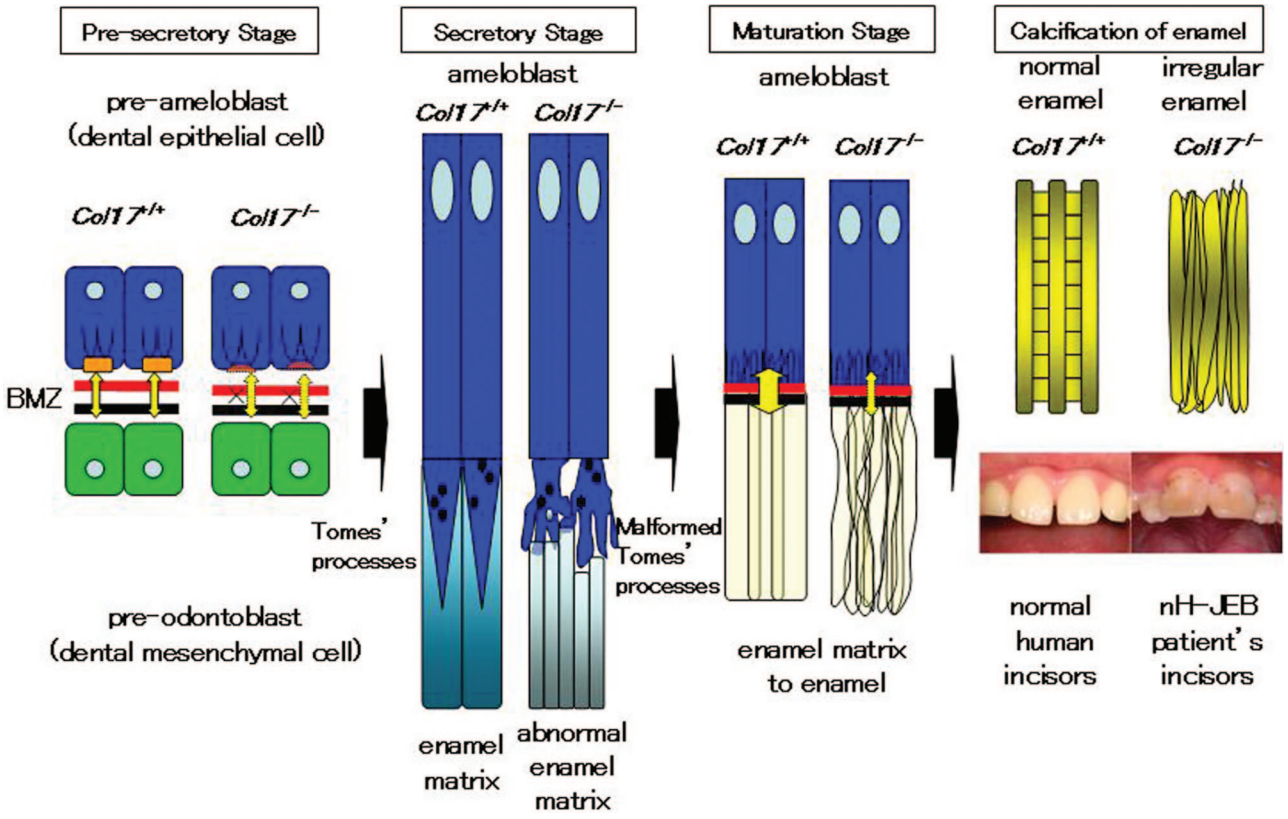

Figure 7. Schemes of normal enamel formation in *Col17*$^{+/+}$ mice and defective enamel formation in *Col17*$^{-/-}$ mice. In the *Col17*$^{+/+}$ incisors (**left**), normal enamel matrix is formed by Tomes' processes, resulting in intact enamel formation. In the *Col17*$^{-/-}$ incisors (**right**), disruptive Tomes' processes produce disturbed enamel matrix, leading to irregular enamel formation.

tologically, strong expression of amelogenin and ameloblastin was seen in the ameloblasts cultured from the *Col17*$^{+/+}$ mice, although expression of both proteins was remarkably weak in cells cultured from the *Col17*$^{-/-}$ mice (Figure 6, C–F).

Discussion

nH-JEB is a hereditary blistering skin disease with tissue separation occurring within the lamina lucida of the epidermal basement membrane zone. nH-JEB is characterized by generalized blistering, alopecia, reduced axillary and public hair, dystrophic nails, and dental abnormalities.[4,15] Molecular genetic studies revealed that nH-JEB is caused by mutations in the genes encoding COL17 or laminin 332.[16] Most nH-JEB patients exhibit enamel hypoplasia, and pitting and coarsening of the tooth surface enamel.[6,7]

The present study revealed that the secretory ameloblasts of the *Col17*$^{-/-}$ mice lacked Tomes' processes and exhibited disturbed enamel matrix secretion, which resulted in imperfect amelogenesis demonstrated by malformed enamel rods and irregular enamel matrix (Figure 7).

Mice only have one set of dentition whereas the human disease nH-JEB affects both primary and secondary dentition. Due to these differences, the tooth abnormalities demonstrated in *Col17*$^{-/-}$ mice are unlikely to be pathophysiologically relevant to the nH-JEB human disease. However, the physiological processes of enamel formation are identical both in human and mouse dentition.[17,18] Thus, we believe that the present *Col17*$^{-/-}$ mice are a practical and useful model in which to study nH-JEB dental abnormalities.

We studied the developmental processes of the teeth in *Col17*$^{-/-}$ mice. The teeth develop through the presecretory, secretory, and maturation stages.[19] At presecretory stage, hypoplasia of hemidesmosomes is the only apparent abnormality in *Col17*$^{-/-}$ mice teeth. In ameloblasts in the secretory stage, disturbed Tomes' process formation was observed in the *Col17*$^{-/-}$ mice, although enamel matrix was seen around the disrupted Tomes' processes. The Tomes' processes are known to be involved in the secretion of enamel matrix.[19]

Ameloblasts at the maturation stage showed no apparent abnormality, although the crystal structure of the enamel matrix was disturbed in the *Col17*$^{-/-}$ mice. Scanning electron microscopy revealed that enamel rods were malformed and irregular in the enamel matrix of the *Col17*$^{-/-}$ mice. These morphological abnormalities were not observed in the rescued COL17-humanized mice and thus it was confirmed that the abnormalities were direct effects of the COL17 deficiency.

Contact microradiography demonstrated that enamelization of the enamel matrix and calcification were delayed in the *Col17*$^{-/-}$ mice. In addition, reduced iron

deposition was revealed in the enamel of *Col17*$^{-/-}$ incisors from their whitish color and scanning electron microscopy-EDX findings. Iron deposition is known to occur according to the maturation of enamel matrix and mineralization. Thus, reduced iron deposition in the *Col17*$^{-/-}$ mouse incisors suggests defects in enamel maturation and/or mineralization. These results clearly indicate that tooth malformation (amelogenesis imperfecta) in *Col17*$^{-/-}$ mice and probably in *COL17*-deficient nH-JEB patients is caused by aberrant differentiation of ameloblasts. These abnormal ameloblasts lacked Tomes' processes and secreted reduced amounts of enamel matrix irregularly, resulting in disturbed enamel matrix, irregular enamelization and calcification (Figure 7).

We ultrastructurally examined teeth from an adult patient with nH-JEB due to COL17 deficiency using scanning electron microscopy. Enamel rods were malformed and the enamel rod inclination was irregularly oriented and disrupted in the enamel layer of the patient's teeth (data not shown). These abnormalities are most likely a consequence of a lack of COL17 causing aberrant ameloblast differentiation, similar to the *Col17*$^{-/-}$ mice, although we cannot completely exclude the possibility that the morphological changes in the nH-JEB patient's teeth were non-specific abnormalities caused by secondary bacterial infection, etc.

It is reported that heterozygous carriers of glycine substitutions in *COL17A1* show dental abnormalities,[7,20] although such dominant negative mutations in *COL17A1* fail to manifest with a blistering skin phenotype.[20] It is considered that abnormal dentition in the heterozygous carriers is a direct result of dominantly inherited glycine substitutions in *COL17A1* with dominant interference between the wild-type and mutant protein causing ameloblast dysfunction and disruption of enamel deposition.[20] In addition, dental abnormalities were seen both in individuals heterozygous for a *COL17A1* nonsense mutation p.Arg1226X[21] and in heterozygous carriers of a *COL17A1* deletion mutation c.823delA.[7] By contrast, in the present study, *Col17*$^{+/-}$ mice showed no apparent tooth abnormality, probably because the critically disruptive *Col17* allele carried by the mice had no dominant negative effect against wild-type COL17 protein.

Ameloblasts cultured without interaction with mesenchymal tissue cannot differentiate sufficiently to form columnar epithelium.[22] Such insufficiently differentiated ameloblasts express tuftelin, but not other enamel proteins, including amelogenin and ameloblastin.

Ameloblasts in *Col17*$^{-/-}$ mice express tuftelin to an extent similar to that of *Col17*$^{+/+}$ mice, *Col17*$^{-/-}$ ameloblasts express reduced amounts of amelogenin and ameloblastin. Tuftelin is known to be expressed by epithelial cells at a very early stage (the pre-secretory ameloblast stage) of odontogenesis,[23,24] although other major enamel proteins are expressed at the secretory stage.[25] Thus, the results of the present enamel protein expression study further support the idea that ameloblast differentiation from the pre-secretory stage to the secretory stage is disturbed in *Col17*$^{-/-}$ mice.

In the *Col17*$^{-/-}$ mice, ameloblast differentiation was retarded, resulting in malformation of Tomes' processes. The present results in *Col17*$^{-/-}$ mice clearly demonstrated that COL17, a component of the hemidesmosome involved in basement membrane adhesion, also regulates differentiation of odontogenic epithelial cells in ameloblasts and plays and essential role in enamelization.

Laminin 332 is known to be an important component of hemidesmosomes and another causative molecule underlying the JEB phenotype. Remarkable abnormalities, including disturbance of ameloblast differentiation and reduced enamel deposition, have also been reported in the incisors of laminin 332-disrupted mice.[8] These facts further support the idea that interactions between ameloblasts and mesenchymal tissue via hemidesmosomes are crucial for ameloblast differentiation and function.[26,27] Ultrastructural changes of Tomes' processes were not described in laminin 332-disrupted *LAMA3*$^{-/-}$ mice. However, the reduced size of secretory ameloblasts reported in *LAMA3*$^{-/-}$ mice suggest absence or hypoplasia of Tomes' processes in *LAMA3*$^{-/-}$ mice, similar to that observed in *Col17*$^{-/-}$ mice. During the maturation stage, tissue organization was completely disrupted in the enamel epithelium of *LAMA3*$^{-/-}$ mice,[8] but not of *Col17*$^{-/-}$ mice. These findings suggest that a lack of COL17 and a lack of laminin 332 have similar negative effects on ameloblast differentiation and enamel formation, although laminin 332 deficiency appears to have more severe disruptive effects on enamel epithelium, compared with COL17 deficiency.

Our results show that disruption of the *Col17* gene leads to abnormal interaction between enamel epithelium and the underlying mesenchyme via the EMJ, resulting in defective ameloblast differentiation. Consequently, the *Col17*$^{-/-}$ mice exhibit ameloblasts with malformed Tomes' processes and the secretion of enamel matrix was diminished at the secretary stage. At the maturation stage, the *Col17*$^{-/-}$ mice show delayed calcification and reduced iron deposition in the enamel. We consider that these mechanisms contribute to the immature and irregular enamel formation seen in *Col17*$^{-/-}$ mice. In conclusion, epithelial-mesenchymal interactions via the EMJ are important for tooth morphogenesis, and hemidesmosome components are thought to regulate the proliferation and differentiation of tooth forming cells including ameloblasts.

Acknowledgments

We thank Prof. James R. McMillan and Dr. Heather A. Long for their revisions and comments and Dr. Yoshinobu Nodasaka, Mr. Yoshiyuki Honma, and Ms. Kaori Sakai for their fine technical assistance on this project.

References

1. Maas R, Bei M: The genetic control of early tooth development. Crit Rev Oral Biol Med 1997, 8:4–39
2. Liu F, Chu EY, Watt B, Zhang Y, Gallant NM, Andl T, Yang SH, Lu MM, Piccolo S, Schmidt-Ullrich R, Taketo MM, Morrisey EE, Atit R, Dlugosz AA, Millar SE: Wnt/beta-catenin signaling directs multiple stages of tooth morphogenesis. Dev Biol 2008, 313:210–224

3. Borradori L, Sonnenberg A: Structure and function of hemidesmosomes: more than simple adhesion complexes. J Invest Dermatol 1999, 112:411–418
4. McGrath JA, Gatalica B, Christiano AM, Li K, Owaribe K, McMillan JR, Eady RA, Uitto J: Mutations in the 180-kD bullous pemphigoid antigen (BPAG2), a hemidesmosomal transmembrane collagen (COL17A1), in generalized atrophic benign epidermolysis bullosa. Nat Genet 1995, 11:83–86
5. Kirkham J, Robinson C, Strafford SM, Shore RC, Bonass WA, Brookes SJ, Wright JT: The chemical composition of tooth enamel in recessive dystrophic epidermolysis bullosa: significance with respect to dental caries. J Dent Res 1996, 75:1672–1678
6. Nakamura H, Sawamura D, Goto M, Nakamura H, Kida M, Ariga T, Sakiyama Y, Tomizawa K, Mitsui H, Tamaki K, Shimizu H: Analysis of the COL17A1 in non-Herlitz junctional epidermolysis bullosa and amelogenesis imperfecta. Int J Mol Med 2006, 18:333–337
7. Murrell DF, Pasmooij AM, Pas HH, Marr P, Klingberg S, Pfendner E, Uitto J, Sadowski S, Collins F, Widmer R, Jonkman MF: Retrospective diagnosis of fatal BP180-deficient non-Herlitz junctional epidermolysis bullosa suggested by immunofluorescence (IF) antigen-mapping of parental carriers bearing enamel defects. J Invest Dermatol 2007, 127:1772–1775
8. Ryan MC, Lee K, Miyashita Y, Carter WG: Targeted disruption of the LAMA3 gene in mice reveals abnormalities in survival and late stage differentiation of epithelial cells. J Cell Biol 1999, 145:1309–1323
9. Nishie W, Sawamura D, Goto M, Ito K, Shibaki A, McMillan J, Sakai K, Nakamura H, Olasz E, Yancey K, Akiyama M, Shimizu H: Humanization of autoantigen. Nat Med 2007, 13:378–383 in-90
10. Tung K, Fujita H, Yamashita Y, Takagi Y: Effect of turpentine-induced feverduring the enamel formation of rat incisor. Arch Oral Biol 2006, 51:464–470
11. Osawa M, Kenmotsu S, Masuyama T, Taniguchi K, Uchida T, Saito C, Ohshima H: Rat wct mutation induces a hypo-mineralization form of amelogenesis imperfecta and cyst formation in molar teeth. Cell Tissue Res 2007, 330:97–109
12. Fukumoto S, Kiba T, Hall B, Iehara N, Nakamura T, Longenecker G, Krebsbach PH, Nanci A, Kulkarni AB, Yamada Y: Ameloblastin is a cell adhesion molecule required for maintaining the differentiation state of ameloblasts. J Cell Biol 2004, 167:973–983
13. Fukumoto S, Yamada A, Nonaka K, Yamada Y: Essential roles of ameloblastin in maintaining ameloblast differentiation and enamel formation. Cells Tissues Organs 2005, 181:189–195
14. Masuya H, Shimizu K, Sezutsu H, Sakuraba Y, Nagano J, Shimizu A, Fujimoto N, Kawai A, Miura I, Kaneda H, Kobayashi K, Ishijima J, Maeda T, Gondo Y, Noda T, Wakana S, Shiroishi T: Enamelin (Enam) is essential for amelogenesis: eNU-induced mouse mutants as models for different clinical subtypes of human amelogenesis imperfecta (AI). Hum Mol Genet 2005, 14:575–583
15. Jonkman MF, de Jong MC, Heeres K, Pas HH, van der Meer JB, Owaribe K, Martinez de Velasco AM, Niessen CM, Sonnenberg A: 180-kD bullous pemphigoid antigen (BP180) is deficient in generalized atrophic benign epidermolysis bullosa. J Clin Invest 1995, 95:1345–1352
16. Varki R, Sadowski S, Pfendner E, Uitto J: Epidermolysis bullosa. I. Molecular genetics of the junctional and hemidesmosomal variants. J Med Genet 2006, 43:641–652
17. Miletich I, Sharpe PT: Normal and abnormal dental development. Hum Mol Genet 2003, 12:R69–R73
18. Fleischmannova J, Matalova E, Tucker AS, Sharpe PT: Mouse models of tooth abnormalities. Eur J Oral Sci 2008, 116:1–10
19. Smith CE: Cellular and chemical events during enamel maturation. Crit Rev Oral Biol Med 1998, 9:128–161
20. McGrath JA, Gatalica B, Li K, Dunnill MG, McMillan JR, Christiano AM, Eady RA, Uitto J: Compound heterozygosity for a dominant glycine substitution and a recessive internal duplication mutation in the type XVII collagen gene results in junctional epidermolysis bullosa and abnormal dentition. Am J Pathol 1996, 148:1787–1796
21. Floeth M, Bruckner-Tuderman L: Digenic junctional epidermolysis bullosa: mutations in COL17A1 and LAMB3 genes. Am J Hum Genet 1999, 65:1530–1537
22. Morotomi T, Kawano S, Toyono T, Kitamura C, Terashita M, Uchida T, Toyoshima K, Harada H: In vitro differentiation of dental epithelial progenitor cells through epithelial-mesenchymal interactions. Arch Oral Biol 2005, 50:695–705
23. Deutsch D, Leiser Y, Shay B, Fermon E, Taylor A, Rosenfeld E, Dafni L, Charuvi K, Cohen Y, Haze A, Fuks A, Mao Z: The human tuftelin gene and the expression of tuftelin in mineralizing and nonmineralizing tissues. Connect Tissue Res 2002, 43:425–434
24. Leiser Y, Blumenfeld A, Haze A, Dafni L, Taylor AL, Rosenfeld E, Fermon E, Gruenbaum-Cohen Y, Shay B, Deutsch D: Localization, quantification, and characterization of tuftelin in soft tissues. Anat Rec 2007, 290:449–454
25. Fukumoto S, Yamada Y: Extracellular matrix regulates tooth morphogenesis. Connect Tissue Res 2005, 46:220–226
26. Yoshiba K, Yoshiba N, Aberdam D, Meneguzzi G, Perrin-Schmitt F, Stoetzel C, Ruch JV and Lesot H: Expression and localization of laminin-5 subunits during mouse tooth development. Dev Dyn 1998, 211:164–176
27. Fukumoto S, Miner JH, Ida H, Fukumoto E, Yuasa K, Miyazaki H, Hoffman MP, Yamada Y: Laminin alpha5 is required for dental epithelium growth and polarity and the development of tooth bud and shape. J Biol Chem 2006, 24;281:5008–5016